Journal of Aerosol Science 67 (2014) 13–20

Contents lists available at ScienceDirect

Journal of Aerosol Science

journal homepage: www.elsevier.com/locate/jaerosci

Bimodal size distribution of primary particles in the plasma of welding fume: Coalescence of nuclei

V.I. Vishnyakov*, S.A. Kiro, A.A. Ennan

Physical-Chemical Institute for Environmental and Human Protection, National Academy of Sciences of Ukraine, 3 Preobrazhenskaya, Odessa 65082, Ukraine

ARTICLE INFO

Article history:
Received 28 June 2013
Received in revised form
8 September 2013
Accepted 24 September 2013
Available online 2 October 2013

Keywords:
Thermal plasma
Welding fume
Nucleation
Coalescence
Particle size distribution
Multimodal distribution

ABSTRACT

Nucleation and growth of the nuclei in the thermal plasma of the ionized metal vapors of welding fume are studied. The coalescence of liquid droplets formed by the vapors' nucleation is calculated. There is a high flow rate of condensable atoms from the gas phase into the condensed phase caused by the nucleation and association of nuclei with the aggregated droplets. The fast association of the nuclei with aggregated droplets leads to a decrease in the condensable vapor supersaturation and to the termination of nucleation and start of the bimodal coalescence. As a result, in the beginning of phase transition, there is bimodal size distribution of the primary particles: the small-size primary particles formed by association between the nuclei (intramodal coalescence only), and the primary large-size particles formed by association between the aggregated droplets and the nuclei (intramodal and intermodal coalescence).

1. Introduction

A low-temperature thermal dusty plasma is an aerosol at atmospheric or higher pressure and at temperatures of 1000–3000 K, which contains easily ionizable atoms of alkali metals as a natural impurity or in the form of specific additional agents. Ionization in a thermal plasma occurs due to collisions between electrons and alkali metal atoms, which are the basic suppliers of free electrons and singly charged positive ions. Therefore, a thermal plasma is strongly collisional unlike a low pressure gas–discharge plasma (Fortov et al., 2004). Examples of thermal collisional plasmas are the combustion plasma, which is formed in flames (Doroshenko et al., 2009; Poletaev & Florko, 2008), and the condensation zone of arc welding fume (Kobayashi et al., 1983). Both kinds of plasma represent ionized gas containing the vapor of metals and/or metal oxides, which are ready to condensate; therefore, as a result of volume condensation, such a plasma contains the dust as liquid droplets and, after the cooling and phase transition, as solid particles.

Such a plasma can be used in the technology of synthesis of nano-sized oxide particles with the required properties (Gonzalez et al., 2008; Kumfer et al., 2010; Seo & Hong, 2012). Thus, a new technology can be developed to obtain new materials. Flexible ceramics is an example of such new materials that can be used to make crucibles for melting metals, gas turbines, liners for jet and rocket motor tubes, resistance furnaces and ultra-high frequency furnaces (Laurvick & Singaraju, 2002). Another application of nano-sized particles is the production of fuel cells. Solid oxide fuel cells differ from other fuel cell technologies, because they are composed of all-solid-state materials, and as a result can operate at temperatures significantly higher than any other category of fuel cells (Singhal & Kendall, 2003).

The formation of condensed particles in the plasma occurs as a result of nucleation and growth of the nuclei (Girshick et al., 1993; LaViolette et al., 1996; Reist, 1984), and this process is strongly dependent on the plasma properties (Vishnyakov, 2008;

* Corresponding author. Tel.: +380 487237528; fax: +380 487231116.
E-mail addresses: drvishnyakov@mail.ru, eksvar@ukr.net (V.I. Vishnyakov).

0021-8502/$ - see front matter © 2013 Elsevier Ltd. All rights reserved.
http://dx.doi.org/10.1016/j.jaerosci.2013.09.007

Vishnyakov et al., 2011). The temperature in the condensation zone is higher than melting point of the condensable matter, therefore the nuclei are in the liquid state. The condensable vapor mixes with air and this vapor–gas mixture cools down, which leads to the beginning of growth of the nuclei. The growth of the nuclei occurs until the temperature reaches the melting point. The phase transition terminates the formation of the primary particles; secondary particles are formed as a result of further coagulation.

The dusty plasma of arc welding fume was investigated by Fuglsang et al. (2011), Asbach et al. (2009) and Brand et al. (2013). It was discovered that the primary particles are described by the bimodal size distribution. The paper by Fuglsang et al. (2011) demonstrated that particles of welding fume, collected by an Electrical Low Pressure Impactor, have a size of the first mode below 10 nm and a size of the second one is about 100 nm. But it should be noted that these particles are not the primary particles. Similar studies of the secondary particles (agglomerates of the primary particles) by Asbach et al. (2009) also demonstrated the bimodal size distribution with sizes of about 10 nm and 100–150 nm. The paper by Brand et al. (2013) presented the number-based size distributions of the particles of welding fume, where three modes can be observed: the particles of the first mode smaller than 6 nm, a size of the second mode is 20–30 nm and a size of the third mode is 100–200 nm. The investigation by Ennan et al. (2013) found two close modes of the secondary particles with sizes of ~200 and ~300 nm, and shown that these secondary particles can be a result of coagulation of the primary particles with sizes of ~2 and ~20 nm. The origin of the first mode is clear, it is the primary particles formed as a result of nuclei' growth. As to the second mode, one may assume that these particles are the result of droplets' coalescence (Tashiro et al., 2010).

This paper deals with the nucleation and growth of the nuclei occurring simultaneously with their coalescence; besides, the exchange processes between the particles and the plasma, where the nucleation occurs, are taken into account. The proposed calculation method allows defining the primary particle size distribution function in any moment of time.

2. Nucleation and growth of nuclei without coalescence

The calculation of heterogeneous ion-induced nucleation in the plasma by taking into account the interphase interaction, when nucleation depends on the electron exchange between the nucleus and the plasma, was done using the procedure suggested by Vishnyakov et al. (2013). The subject of modeling is the dusty plasma formed during cooling of the iron vapor stream from the temperature of 3000 K down to the melting point of iron (1800 K) as a result of mixing with the air. The vapor–gas mixture contains iron atoms and alkali metals as ionizable atoms in the following ratio: $g_{Fe} = 0.36$, $g_K = 0.06$, $g_{Na} = 0.03$, where g is the part by weight (the system under consideration corresponds to the plasma of shielded metal arc welding fume, Oprya et al., 2012).

The presence of the alkali metal atoms provides the content of ions with the equilibrium number density from $3.6 \times 10^{15}\,\mathrm{cm}^{-3}$ (atom density is $1.8 \times 10^{18}\,\mathrm{cm}^{-3}$), at the temperature of 3000 K, to $7.5 \times 10^{12}\,\mathrm{cm}^{-3}$ (atom density is $1.2 \times 10^{18}\,\mathrm{cm}^{-3}$), at the temperature of 1800 K. But real ion number density is less, because ions are the nucleation centers; for example at the temperature of 1800 K their number density is $5 \times 10^{12}\,\mathrm{cm}^{-3}$ (atom density is $6.5 \times 10^{17}\,\mathrm{cm}^{-3}$, i.e. about $5.5 \times 10^{17}\,\mathrm{cm}^{-3}$ atoms of alkali metals via ionization became a nucleus center). In the used procedure the ionization of alkali metal atoms due to the collisions and UV-radiation from the arc is considered. The electrons appear in the system not only due to the atoms' ionization, the thermionic emission and photoemission from the particles are also considered in the procedure. Therefore, the number of electron can be more than a number of ions, if the particles did not accumulate the major part of electrons. For example, at the temperature of 1800 K, the electron number density is $5.4 \times 10^{12}\,\mathrm{cm}^{-3}$.

As the vapor stream mixes with the air, the partial pressures of condensable vapors (P_i) in the vapor–gas mixture and their supersaturations ($S_i = P_i/P_{i,sat}$) can be calculated using the temperature and the vapor composition:

$$P_i = \frac{\delta m_i/\mu_i}{\delta m_0/\mu_0 + \delta m_{air}/\mu_{air}} P, \tag{1}$$

where $\delta m_i = g_i \delta m_0$ is the flow rate of the ith component; $\delta m_0 = 10^{-2}$ g/s is the mass flow rate of the vapors stream; μ_i is the atomic mass of the ith component; $\mu_0 = 26$ g/mol is the effective atomic mass of the vapors stream, μ_{air} is the air molecular mass; $P = 1.01 \times 10^5$ Pa is the atmospheric pressure; δm_{air} is the mass rate of entrainment of the air by the vapor stream, which is defined by the current temperature of the vapor–gas mixture T, the temperature of the environment $T_\infty \sim 300$ K and the initial temperature $T_0 \sim 3000$ K:

$$\delta m_{air} = \frac{T_0 - T}{T - T_\infty} \delta m_0. \tag{2}$$

The current total number density of iron atoms in the vapor without account of the condensed phase is determined using (1) via the perfect–gas relation:

$$N_{a0} = \frac{P_{Fe}}{k_B T}, \tag{3}$$

where k_B is the Boltzmann constant. Adjusted to take into account that some iron atoms are in the condensed phase, the number density of the iron atoms remaining in the gas phase is

$$N_a = N_{a0} - N_{ac},$$

where $N_{ac} = n_a N_d$ is the number density of the iron atoms in the condensed phase; N_d is the number density of the droplets of nuclei or aggregates; $n_a = 4\pi\rho_c r_d^3/3m_c$ is the average number of atoms in the droplet; r_d is the droplet radius; ρ_c is the density of the condensable matter; m_c is the atomic mass of the condensable matter (iron).

The nuclei are in the equilibrium with the environment and cannot grow, until there is a potential barrier of growth activation which decreases when the supersaturation of condensable vapor increases during cooling (Kuni et al., 2001). After the activation barrier disappears, the growth of the nuclei is determined by the increment of the mass with regard to the difference between the absorption and transpiration fluxes (Fuchs, 1964):

$$\frac{dm_d}{dt} = \pi r_d^2 \alpha_c v_{Ta} m_c (N_a - N_s)$$

where α_c is the condensation factor; $v_{Ta} = \sqrt{8k_B T/\pi m_a}$ is the thermal velocity of the condensable atoms; $N_s = N_a S_R/S$ is the number density of the condensable atoms near the droplet surface; S is the current supersaturation; $S_R = P_{sat}(r_d)/P_{sat}(\infty)$ is the change in vapor pressure due to surface curvature and exchange interaction, as defined by the modernized Kelvin equation by taking into account the droplets charge (Vishnyakov et al., 2013):

$$\ln(S_R) = \frac{m_c}{4\pi\rho_c k_B T}\left[8\pi\gamma\frac{r_d + 3\delta}{(r_d + 2\delta)^2} - \frac{e^4\tilde{Z}_d^3}{3k_B T r_d^5} - \frac{\tilde{Z}_d W_d}{r_d^3} - \frac{e^2(1 + Z_0^2 - \tilde{Z}_d^2)}{2r_d^4}\right],$$

γ is the surface free energy of the flat surface; δ is the Tolmen length (Bahadur & Ressell, 2008); W_d is the electronic work function; $\tilde{Z}_d$ is the droplet charge with respect to the charge of environment (the total droplet charge is $Z_d = Z_0 + \tilde{Z}_d$); Z_0 is the charge of environment, which is equal, but with opposite sign, to the volume charge of the gas phase per one droplet.

Then, change in the radius of increased nucleus' droplet is described by the following equation:

$$\frac{dr_d}{dt} = \frac{\alpha_c v_{Ta} m_c}{4\rho_c} N_a \left(1 - \frac{S_R}{S}\right). \tag{4}$$

The results of modeling of the heterogeneous ion-induced nucleation of iron and growth of the nuclei in the plasma are presented in Fig. 1. The evolution of processes is considered during cooling of the vapor–gas mixture from the temperature of 2380 K ($t=0$) down to the temperature of 1800 K at the rate of 1 K/μs. The time step was chosen $dt = 1$ μs, because the Maxwell relaxation time, which determines the stabilization of the diffusion–drift balance, is $\tau_M \sim 0.1$–1 μs in such systems (Vishnyakov, 2005). It has allowed calculating the equilibrium state of environment in each step.

The iron nucleation begins at the temperature of ~2340 K, when the vapor supersaturation reaches the value $S=5.3$. The supersaturation reaches the value $S=6.5$ at the temperature of ~2310 K, and growth of the nuclei begins. The great number of iron atoms is condensed, therefore the supersaturation falls down to value $S=2.8$ and decreases as the droplets grow up to radius $r_d \sim 1$ nm. The nuclei number density increases till growth starts and remains stationary at $N_d \sim 10^{15}$ cm^{-3}. The iron atom number density in the gas phase decreases as some atoms turn into the condensed phase and vapors are diluted by the air. As a result, in the beginning of phase transition, the iron content in the gas phase is much less than that in the condensed phase.

3. Coalescence: solution techniques using the method of moments

The large number density of nuclei $N_d \sim 10^{15}$ cm^{-3} causes their intensive collisions due to the Brownian motion, and coalescence, as they are in the liquid state. The evolution of the number density of stable droplets of size j by coalescence

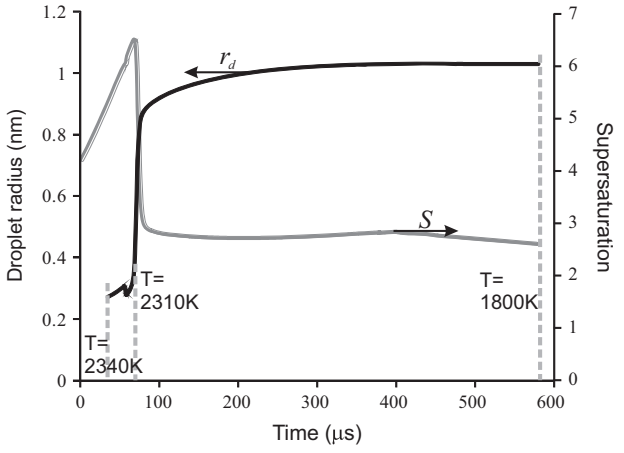

Fig. 1. Evolution of the droplet average radius r_d and supersaturation of iron vapor S.

due to the Brownian motion is described by the Smoluchowski balance equation (Bilodeau & Proulx, 1996):

$$\frac{\partial N_j}{\partial t} = \frac{1}{2}\sum_{i=1}^{j-1} \beta(i,j-i) N_i N_{j-i} - N_j \sum_{i=1}^{\infty} \beta(i,j) N_i,$$

where $\beta(i,j)$ is the collision kernel.

As a result the aggregated droplets with the average diameter $d_d = (6m_c\overline{n}/\pi\rho_c)^{1/3}$ are formed, where $\overline{n}$ is the average number of the atoms in a new droplet, which increases while the coalescence occurs. However, it is necessary to take into account that the nucleation continues until there exists a sufficient density of the condensable matter. Thus, already at the initial stage of condensation the bimodal size distribution of the droplets occurs. The first mode contains the droplets of nuclei, the second mode is represented by aggregated droplets resulting from the long-term coalescence.

The equation of the iron atoms conservation is as follows:

$$N_{ac} = \overline{n}_1 N_{d1} + \overline{n}_2 N_{d2}, \tag{5}$$

where $\overline{n}_1$ and $\overline{n}_2$ are the average numbers of atoms in the droplets of the first and second modes respectively; N_{d1} and N_{d2} are the droplet number densities in the first and second modes, respectively (if it is assumed that the first mode contains nuclei only, then $\overline{n}_1 = n_a$).

When droplets have grown through coalescence, they are described by a log-normal size distribution. It can consider the distribution based on the number of atoms contained in the droplets, using probability density function:

$$f_{ni} = \frac{N_{di}}{n \ln \sigma_i \sqrt{2\pi}} \exp\frac{-(\ln n - \ln n_{0i})^2}{2 \ln^2 \sigma_i} \quad (i = 1,2), \tag{6}$$

and the total distribution function is the superposition of these two: $f_n = f_{n1} + f_{n2}$ (Seigneur et al., 1986). Here $n_{0i} = \overline{n}_i \exp(-\ln^2 \sigma_i/2)$ is the median of distribution; σ_i is the standard deviation.

At the initial moment that corresponds to the nucleation beginning, only one mode consisting of the monodisperse nuclei is formed; and $\sigma = 1$ should be taken into account in Eq. (6), in order to describe the monodisperse nuclei. But a zero value of $\ln \sigma$ is not suitable for the calculations, therefore it can be considered as $\sigma_1 = 1.01$ and $\ln \sigma_1 = 0.01$. The calculations demonstrated that for all values of $\ln \sigma < 0.05$ the results are identical, because right after the first collisions, the mode of the aggregated droplets is formed, and the standard deviation rapidly increases. So, the bimodal distribution occurs as the nucleation continues.

The evolution of such a system can be described by the integral moments of the distribution (6) (Chan et al., 2010; Estrada & Cuzzi, 2008; Whitby & McMurry, 1997). The numerical calculation of the coagulation of particles is the complex problem. Therefore, Cohen & Vaughan (1971) proposed the approximation method based on the moments of size distribution. The moments are described by the following equation:

$$M(k) = \int_0^{\infty} n^k f_n \, dn. \tag{7}$$

The zeros moment represents the total number density of the generated particles, while the first moment corresponds to the total number of atoms in these. The second moment is proportional to the light scattered by the particles in the case where their size is much smaller than the wavelength of the incident light (Colombo et al., 2012).

In this case the Smoluchowski equation is transformed into the following equation (Yu et al., 2008):

$$\frac{\partial M(k)}{\partial t} = \frac{1}{2}\int_0^{\infty} f_n \int_0^{\infty} \beta(n,m) f_m \left[(n+m)^k - n^k - m^k\right] dm \, dn, \tag{8}$$

where n and m are the numbers of atoms in the colliding droplets; $\beta(n,m)$ is the collision kernel. The Brownian collision kernel can be determined by the kinetic theory of gases, or by the diffusion theory according to the droplet size. If the droplets are much smaller than mean free path length of the gas molecules, the kinetic theory of gases must be used to determine the collision kernel:

$$\beta(n,m) = \beta_0 (n^{1/3} + m^{1/3})^2 \sqrt{\frac{n+m}{nm}}, \quad \beta_0 = \left(\frac{3m_c}{4\pi\rho_c}\right)^{1/6} \sqrt{\frac{6k_B T}{\rho_c}}.$$

For the bimodal system, where $f_n = f_{n1} + f_{n2}$, Eq. (8) can be transformed into the two equations

$$\frac{\partial M_1(k)}{\partial t} = \frac{1}{2}\int_0^{\infty} f_{n1} \int_0^{\infty} \beta(n,m) f_{m1} (n+m)^k \, dm \, dn - \int_0^{\infty} f_{n1} n^k \int_0^{\infty} \beta(n,m)(f_{m1} + f_{m2}) \, dm \, dn, \tag{9}$$

$$\frac{\partial M_2(k)}{\partial t} = \int_0^{\infty} \left(f_{n1} + \frac{1}{2} f_{n2}\right) \int_0^{\infty} \beta(n,m) f_{m2} (n+m)^k \, dm \, dn - \int_0^{\infty} (f_{n1} + f_{n2}) \int_0^{\infty} \beta(n,m) f_{m2} m^k \, dm \, dn, \tag{10}$$

where (9) corresponds to the mode of the nuclei and (10) corresponds to the mode of the aggregated droplets.

A moment $M(0)$ defines the droplet number density N_d in the mode:

$$\frac{\partial M_1(0)}{\partial t} = -\frac{1}{2}\int_0^{\infty} f_{n1} \int_0^{\infty} \beta(n,m) f_{m1} \, dm \, dn - \int_0^{\infty} f_{n1} \int_0^{\infty} \beta(n,m) f_{m2} \, dm \, dn, \tag{11}$$

$$\frac{\partial M_2(0)}{\partial t} = -\frac{1}{2}\int_0^\infty f_{n2}\int_0^\infty \beta(n,m) f_{m2}\, dm\, dn, \tag{12}$$

and, as it follows from (11) and (12), the droplet number decreases due to coalescence in both modes; the number of aggregated droplets decreases due to the intramodal coalescence (12), and the number of droplets in the nuclei mode (11) decreases not only due to the intramodal coalescence, but also due to the intermodal association between the nuclei and the aggregated droplets.

A moment $M(1)$ defines the total number of atoms $\overline{n}N_d$ in the mode:

$$\frac{\partial M_1(1)}{\partial t} = -\int_0^\infty f_{n1} n \int_0^\infty \beta(n,m) f_{m2}\, dm\, dn, \tag{13}$$

$$\frac{\partial M_2(1)}{\partial t} = \int_0^\infty f_{n1} n \int_0^\infty \beta(n,m) f_{m2}\, dm\, dn, \tag{14}$$

and, as it follows from (13) and (14), the number of atoms decreases in the first mode and increases in the second mode due to the association between the nuclei and the aggregated droplets. It should be noted that at the usual unimodal coagulation $\partial M(1)/\partial t = 0$.

A moment $M(2)$ allows determining the standard deviation:

$$\frac{\partial M_1(2)}{\partial t} = \int_0^\infty f_{n1} n \int_0^\infty \beta(n,m) f_{m1} m\, dm\, dn - \int_0^\infty f_{n1} n^2 \int_0^\infty \beta(n,m) f_{m2}\, dm\, dn, \tag{15}$$

$$\frac{\partial M_2(2)}{\partial t} = \int_0^\infty f_{n2} n \int_0^\infty \beta(n,m)(2f_{m1} + f_{m2}) m\, dm\, dn + \int_0^\infty f_{n2}\int_0^\infty \beta(n,m) f_{m1} m^2\, dm\, dn, \tag{16}$$

and the average number of atoms in the droplets is

$$\overline{n}_i = \frac{M_i(1)}{M_i(0)}, \tag{17}$$

the standard deviation is defined by the following equation:

$$\ln^2 \sigma_i = \ln\frac{M_i(2) M_i(0)}{M_i(1)^2}. \tag{18}$$

Equations (11)–(18) allow us to completely describe the evolution of the coalescence in the bimodal system of droplets by taking into account both the intramodal coalescence and the intermodal association of droplets of different modes. The Mathcad prime program for calculation was used (Appendix A). At first, the equilibrium state of environment is calculated, i. e. the number densities of the atoms, ions, electrons, and charges of droplets are defined. After that the coalescence is calculated. The time for which the number of droplets decreases twice is $(2\beta_0 \times 10^{15}\ \mathrm{cm}^{-3})^{-1} \sim 8\ \mu\mathrm{s}$ at the temperature of 2000 K. Therefore, the calculation time step of 0.1 μs corresponds to much smaller changes of the number of droplets due to the coalescence. As the calculation time step of the system equilibrium state is 1 μs, the cycle from 10 consecutive calculations of the moments was used in each step of the main program.

4. Nucleation and growth of nuclei with coalescence

The bimodal coalescence of droplets assumes that the first mode of the nuclei associates with the second mode of the aggregated droplets. However, the system thermodynamics requires the presence of the nuclei with equilibrium number density. Therefore, the first mode cannot change, because the new nuclei appear. Thus, the nucleation is the original "pump" for the transfer of the atoms from the gas phase into the aggregated droplets (see (14)), and the intensity of this process is higher than the intensity of the vapor condensation on the aggregated droplets (see (4)). While nucleation takes place, the first mode remains as a monodisperse aerosol, i.e. modeled by the log-normal distribution with the standard deviation $\sigma_1 = 1.01$, and the median $n_{01} = (4\pi\rho_c r_n^3/3m_c)\exp[-(\ln^2\sigma_1)/2]$, where r_n is the nucleus radius.

The second mode changes according to Eqs. (11)–(18). The evolution of the supersaturation and the average radii of droplets is presented in Fig. 2; the evolution of the increment of droplet radii and the droplet charges is presented in Fig. 3. The coalescence leads to the fast growth of the aggregated droplet sizes (curve r_{d2}, Fig. 2) that causes the deceleration in growth of the iron vapor supersaturation (curve S). As a result, the nucleation is prolonged down to the temperature of ~2260 K. Some part of the nuclei "is pumped out" into the second mode, and some part of nuclei should remain as separate droplets in order to keep the system in equilibrium, i.e. to keep the monodisperse state of the first mode (curve r_n, Fig. 2).

The supersaturation falls down to value $S=0.8$ and the nucleation stops. Further the bimodal coalescence occurs, because the requirement for existence of the nuclei as separate droplets disappears. Simultaneously with coalescence there is a growth or evaporation (for the first mode) of droplets (see Fig. 3), in conformity to Eq. (4). This process leads to the integration of the first mode up to average droplet radius $r_{d1} \sim 0.6$ nm and the increase of the standard deviation up to $\sigma_1 = 2.1$.

The charge of droplets and charge of environment influence the rate of the condensation growth (4). In the system under consideration the droplets have negative charges and charge of environment $Z_0 > 0$. An increase of the negative charge of droplets leads to the decrease of their growth rate, as the calculation demonstrated, but an increase of the positive charge of environment leads to the increase of the growth rate. In the present case the absolute value of the negative charge of

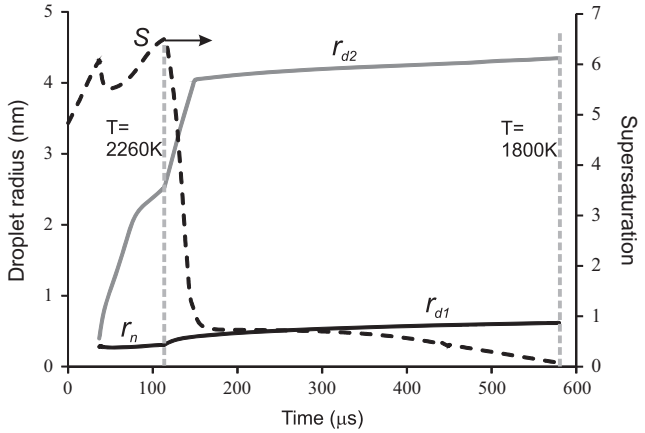

Fig. 2. Evolution of the nucleus radius r_n, the coalescent droplet radii r_{d1}, r_{d2} and the iron vapor supersaturation S.

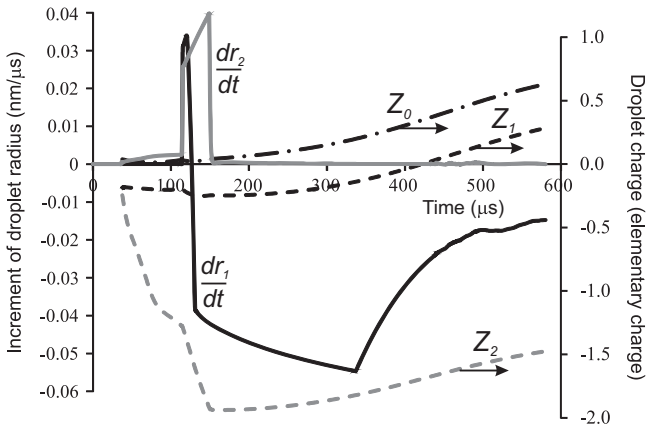

Fig. 3. Evolution of the increment of droplet radii dr_1, dr_2, the droplet charges Z_1, Z_2 and the charge of environment Z_0.

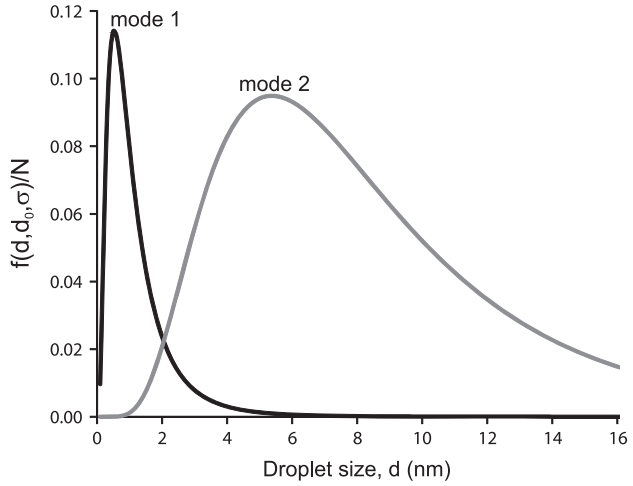

Fig. 4. Log-normal size distribution of the primary particles, normalized on the total particle number.

droplets is more than the charge of environment, therefore the resulting influence of charging reduces the growth rate. It should be noted that the negative charge of the first mode increases the droplet evaporation, but the evaporation rate decreased when the charge becomes positive (see Fig. 3).

The charging of the droplets also affects the collisional cross-section and must influence the coalescence. In the paper by Belov et al. (2000) the ratio of the coagulation kernels of the charged and uncharged particles is defined. The calculations for the system under consideration demonstrated that this ratio is equal to 0.994 for intermodal coalescence, and is equal to

0.999 and 0.94 for intramodal coalescence of the first and second modes, respectively. So, the influence of droplets' charging can be neglected, because their sizes and charges are very small (the screening length is about 500 nm).

The droplets, in the beginning of phase transition, when they become the primary particles, have the bimodal size distribution, presented in Fig. 4. The average diameter of the primary particles of the first mode is $d_1 = 1.2$ nm with the standard deviation $\sigma_1 = 2.1$; the average diameter of the primary particles of the second mode is $d_2 = 8.7$ nm with the standard deviation $\sigma_2 = 1.8$. Further coagulation of the solid primary particles only occurs.

5. Conclusion

The bimodal size distribution of the primary particles can be caused by the coalescence of the nuclei. The aggregated droplets grow, preferentially, by association with the nuclei. As a result of lasting nucleation and association between nuclei and aggregated droplets the intensive transfer of condensable atoms from the gas phase into the condensed phase occurs.

The fast growth of the aggregated droplets leads to the decrease of supersaturation and, as a result, the formation of new nuclei terminates and the first mode starts to grow due to the coalescence of the previously formed nuclei. The nuclei coalescence is accompanied by their evaporation. Thus, two modes of the droplets are formed in the system. The first mode is the droplets of associated nuclei; the second mode is the droplets formed by association between the nuclei and the aggregates.

As a result, after the phase transition, there is the bimodal distribution of the spherical solid primary particles: the particles with the average size of $\sim$1 nm, and the particles with the average size of $\sim$10 nm.

Unfortunately, there is very few direct measuring of the sizes of primary particles in welding fume; only already mentioned (Brand et al., 2013) and also the paper by Richman et al. (2011) represented the particles with the average diameter of 6.5 nm. But the similar system of flame found the particles with the average diameter of 2.7 nm (Strobel et al., 2004). It should be hoped that development of the measuring technique will allow defining the particles with the size of 1 nm.

Appendix A. Algorithm for calculation in Mathcad prime

Here *Rd* is the droplet radius; *Nd* is the droplet number density; σ is the standard deviation; *Rcr* is the radius of the metastable nuclei; *Na* is the number density of condensable iron atoms; *S* is the supersaturation; *Ni* is the ion number density; *Ne* is the electron number density; Z_0 is the charge number of the background; *Z* is the charge number of the droplets; *Environment*() is the subprogram for calculation of the thermodynamic parameters of the plasma, where nucleation and growth of the nuclei occur; *Charge*() is the subprogram for calculation of the charges of the droplets and the charge of the background; *Nucleation*() is the subprogram for calculation of the nucleation; *Growth*() is the subprogram for calculation of the growth of droplets by Eq. (4); *PumpCoalescence*() is the subprogram for calculation of the intermodal coalescence and the intramodal coalescence of the aggregated droplets' mode (the first mode of nuclei does not change); *BimodalCoalescence*() is the subprogram for calculation of the intermodal coalescence and the intramodal coalescence of both nuclei' mode and aggregated droplets' mode.

$T_{start} \leftarrow 2380$ K; $T_{end} \leftarrow 1800$ K; $dt \leftarrow 1$ μs

$v_T \leftarrow 1$ K/μs; $NT \leftarrow \mathrm{ceil}\left(\frac{T_{start} - T_{end}}{v_T \cdot dt}\right)$

$Rd_1, Nd_1, Rd_2, Nd_2 \leftarrow 0$; $Rcr \leftarrow 1$

for i $\in$ **0**...**NT**

  $t \leftarrow i \cdot dt$

  $T \leftarrow T_{start} - v_T \cdot t$

  $Na, Ni, S \leftarrow Environment(T, Rd_1, Nd_1, Rd_2, Nd_2)$

  $Ne, Z_0, Z_1, Z_2 \leftarrow Charge(T, Ni, Rd_1, Nd_1, Rd_2, Nd_2)$

  if $\mathbf{Rd_1} < \mathbf{Rcr}$

    $Rd_1, Nd_1, Rcr \leftarrow Nucleation(T, Na, S, Ne, Z_0)$

    $Rd_2, Nd_2, \sigma_2 \leftarrow PumpCoalescence(T, Rd_1, Nd_1, Rd_2, Nd_2)$

    if $\mathbf{Rd_2} \geq \mathbf{Rcr}$

      $dR \leftarrow Growth(T, Na, S, Z_0, Z_2, Rd_2)$

      $Rd_2 \leftarrow Rd_2 + dR$

    else

      $dR \leftarrow Growth(T, Na, S, Z_0, Z_1, Rd_1)$

      $Rd_1 \leftarrow Rd_1 + dR$

      $Rd_1, Nd_1, \sigma_1, Rd_2, Nd_2, \sigma_2 \leftarrow BimodalCoalescence(T, Rd_1, Nd_1, Rd_2, Nd_2)$

      $dR \leftarrow Growth(T, Na, S, Z_0, Z_2, Rd_2)$

      $Rd_2 \leftarrow Rd_2 + dR$

References

Asbach, Ch., John, A.C., Kaminski, H., & Kuhlbusch, T.A.J. (2009). Ultrafine particles in welding fume. In: *International Seminar on Exposure to ultrafine particles in welding fumes*, February 2009, Hannover. Available at ⟨http://www.bghm.de/fileadmin/user_upload/Arbeitsschuetzer/Fachinformationen/Schweissen/Tagungsband.pdf⟩.

Bahadur, R., & Ressell, L.V. (2008). Effect of surface tension from MD simulations on size-dependent deliquescence of NaCl nanoparticles. *Aerosol Science and Technology*, *42*, 369–376.

Belov, I.A., Ivanov, A.S., Ivanov, D.A., Pal', A.F., Starostin, A.N., Filippov, A.V., Dem'yanov, A.V., & Petrushevich, Yu.V. (2000). Coagulation of charged particles in a dusty plasma. *Journal of Experimental and Theoretical Physics*, *90*, 93–101.

Bilodeau, J.-F., & Proulx, P. (1996). A mathematical model for ultrafine iron powder growth in a thermal plasma. *Aerosol Science and Technology*, *24*, 175–189.

Brand, P., Lenz, K., Reisgen, U., & Kraus, T. (2013). Number size distribution of fine and ultrafine particles from various welding processes. *Annals of Occupational Hygiene*, *57*, 305–313.

Chan, T.L., Liu, Y.H., & Chan, C.K. (2010). Direct quadrature method of moments for the exhaust particle formation and evolution in the wake of the studied ground vehicle. *Journal of Aerosol Science*, *41*, 553–568.

Cohen, E.R., & Vaughan, E.U. (1971). Approximate solution of the equations for aerosol agglomeration. *Journal of Colloid and Interface Science*, *35*, 612–623.

Colombo, V., Ghedini, E., Gherardi, M., Sanibondi, P., & Shigeta, M. (2012). A two-dimensional nodal model with turbulent effects for the synthesis of Si nano-particles by inductively coupled thermal plasmas. *Plasma Sources Science and Technology*, *21*, 025001 (1–12).

Doroshenko, J.A., Poletaev, N.I., & Vishnyakov, V.I. (2009). Dispersion of dust sizes in the plasma of aluminium dust flame. *Physics of Plasmas*, *16*, 094504 (1-3).

Ennan, A.A., Kiro, S.A., Oprya, M.V., & Vishnyakov, V.I. (2013). Particle size distribution of welding fume and its dependency on conditions of shielded metal arc welding. *Journal of Aerosol Science*, *64*, 103–110.

Estrada, P.R., & Cuzzi, J.N. (2008). Solving the coagulation equation by the moments method. *The Astrophysical Journal*, *682*, 515–526.

Fortov, V.E., Khrapak, A.G., Khrapak, S.A., Molotkov, V.I., & Petrov, O.F. (2004). Dusty plasmas. *Physics-Uspekhi*, *47*, 447–492.

Fuchs, N.A. (1964). *Mechanics of aerosols*. Pergamon Press: New York.

Fuglsang, K., Gram, L.K., Markussen, J.B., & Kristensen, J.K. (2011). Measurement of ultrafine particles in emissions from welding processes. In: *16th international conference on joining of materials*, May 2011, Elsinore, Denmark. Available at ⟨http://www14.force.dk/resources/3878.pdf⟩.

Girshick, S.L., Chiu, C.-P., Muno, R., Wu, C.Y., Yang, L., Singh, S.K., & McMurry, P.H. (1993). Thermal plasma synthesis of ultrafine iron particles. *Journal of Aerosol Science*, *24*, 367–382.

Gonzalez, N.Y.M., Morsli, M.E., & Proulx, P. (2008). Production of nanoparticles in thermal plasmas. *Journal of Thermal Spray Technology*, *17*, 533–550.

Kobayashi, M., Maki, S., Hashimoto, Y., & Suga, T. (1983). Investigations on chemical composition of welding fume. *Welding Journal*, *62*, 190-s–196-s.

Kumfer, B.M., Shinoda, K., Jeyadevan, B., & Kennedy, I.M. (2010). Gas-phase flame synthesis and properties of magnetic iron oxide nanoparticles with reduced oxidation state. *Journal of Aerosol Science*, *41*, 257–565.

Kuni, F.M., Shchekin, A.K., & Grinin, A.P. (2001). Theory of heterogeneous nucleation for vapor undergoing a gradual metastable state formation. *Physics-Uspekhi*, *44*, 331–370.

LaViolette, R.A., Berry, R.A., & McGraw, R. (1996). Homogeneous nucleation of metals in a plasma-quench reactor. *Plasma Chemistry and Plasma Processing*, *16*, 250–264.

Laurvick, C.A., Singaraju, B. (2002). The promise of nanotechnology to the world of aerospace. In: *Proceedings of the 21st digital avionics systems conference* (Vol. 2, pp. 9A3-1–9A3-10). Piscataway, NJ: IEEE.

Oprya, M., Kiro, S., Worobiec, A., Horemans, B., Darchuk, L., Novakovic, V., Ennan, A., & Van Grieken, R. (2012). Size distribution and chemical properties of welding fumes of inhalable particles. *Journal of Aerosol Science*, *45*, 50–57.

Poletaev, N.I., & Florko, A.V. (2008). Spectral studies of the gas component of an aluminum dust flame. *Combustion, Explosion, and Shock Waves*, *44*, 437–443.

Reist, P.C. (1984). *Introduction to aerosol science*. Macmillan Publishing: New York.

Richman, J.D., Livi, K.J.T., & Geyh, A.S. (2011). A scanning transmission electron microscopy method for determination of manganese composition in welding fume as a function of primary particles size. *Journal of Aerosol Science*, *42*, 408–418.

Seigneur, C., Hudischewskyj, A.B., Seinfeld, J.H., Whitby, K.T., Whitby, E.R., Brock, J.R., & Barnes, H.M. (1986). Simulation of aerosol dynamics: A comparative review of mathematical models. *Aerosol Science and Technology*, *5*, 205–222.

Seo, J.H., & Hong, B.G. (2012). Thermal plasma synthesis of nano-sized powders. *Nuclear Engineering and Technology*, *44*, 9–20.

Singhal, S.C., & Kendall, K. (2003). *High-temperature solid oxide fuel cells*. Elsevier: New York.

Strobel, R., Krumeich, F., Stark, W.J., Pratsinis, S.E., & Baiker, A. (2004). Flame spray synthesis of Pd/Al_2O_3 catalysts and behavior in enantioselective hydrogenation. *Journal of Catalysis*, *222*, 307–314.

Tashiro, S., Zeniya, T., Yamamoto, K., Tanaka, M., Nakata, K., Murphy, A.B., Yamamoto, E., Yamazaki, K., & Suzuki, K. (2010). Numerical analysis of fume formation mechanism in arc welding. *Journal of Physics D: Applied Physics*, *43*, 434012 (1–12).

Vishnyakov, V.I. (2005). Interaction of dust grains in strong collision plasmas: Diffusion pressure of nonequilibrium charge carriers. *Physics of Plasmas*, *12*, 103502 (1–6).

Vishnyakov, V.I. (2008). Homogeneous nucleation in thermal dust-electron plasmas. *Physical Review E*, *78*, 056406 (1–5).

Vishnyakov, V.I., Kiro, S.A., & Ennan, A.A. (2011). Heterogeneous ion-induced nucleation in thermal dusty plasmas. *Journal of Physics D: Applied Physics*, *44*, 215201 (1–7).

Vishnyakov, V.I., Kiro, S.A., & Ennan, A.A. (2013). Formation of primary particles in welding fume. *Journal of Aerosol Science*, *58*, 9–16.

Whitby, E.R., & McMurry, P.H. (1997). Modal aerosol dynamics modeling. *Aerosol Science and Technology*, *27*, 673–688.

Yu, M., Lin, J., & Chan, T. (2008). A new moment method for solving the coagulation equation for particles in Brownian motion. *Aerosol Science and Technology*, *42*, 705–713.